Effect of size and shape dispersion on the averaged magnetic response of ensembles of semiconductor quantum rings

L. M. Thu, W. T. Chiu, and O. Voskoboynikov*

Department of Electronic Engineering and Institute of Electronics, National Chiao Tung University, Hsinchu 30010, Taiwan

(Received 5 November 2011; revised manuscript received 6 March 2012; published 11 May 2012)

In this paper a theoretical study was made of the conditional averages of the magnetization and magnetic susceptibility of dispersive ensembles of nano-objects with a very complex geometry—self-assembled wobbled semiconductor quantum rings. Using the multivariate statistics approach and previously proposed mapping method the impact of the dispersion of the ring geometry parameters on the static magnetic response of the ensembles has been investigated near the first Aharonov-Bohm oscillation. The description is suited to clarify the important question of which geometrical parameters' dispersions are crucial for the formation and properties of the magnetic response of ensembles. We theoretically show that for the dispersive ensembles of InGaAs/GaAs capped wobbled quantum rings the actual value and temperature dependence of the differential magnetic susceptibility can be optimized by an appropriate control of the conditional parameters of the ensembles. The ring rim radius variations play a crucial role in this dependence. We have managed to simulate in detail the temperature behavior of the meaningful averages of the magnetization and positive peak of the differential magnetic susceptibility for ensembles of the rings known from the experiment. The simulated temperature dependence, position, and magnitude of the positive peak in the differential magnetic susceptibility are in a good agreement with the experimental observations.

DOI: 10.1103/PhysRevB.85.205419 PACS number(s): 73.21.−b, 73.21.La, 78.67.Hc

I. INTRODUCTION

Recent advances in lithography, colloidal chemistry, and epitaxial growth have made it possible to produce semiconductor nano-objects (quantum dots, quantum dot molecules, quantum dot posts, quantum rings, etc.) within a wide range of material parameters and geometrical shapes, investigate their properties in details, and use them for various novel applications (see, e.g., Refs. 1–5 and references therein). It is well known that the effectiveness of applications of the nano-objects is limited by their material and structural uniformity. At the same time, geometrical and material parameters' dispersion (shapes, sizes, and material compositions) is the inherent property of the contemporary self-assembled semiconductor nano-objects (see, e.g., Refs. 6–9). The dispersion leads to fluctuations in the demanded properties of macrosystems (ensembles) combined from the nano-objects. For instance, to perform large-scale quantum information processing we have to assemble macrosystems from many uniform and regular nanosized elements. The dispersion in the nano-objects' parameters results in the noncontrollable decoherence in the entanglement of multiquantum bits. The same requirements are of the paramount importance in nano-optics and nanomedicine. The dispersion leads to the inhomogeneous broadening in optical spectra which can drastically decrease applicability of the integrated optical systems. In this respect the most interesting and challenging goal is to formulate statistical models ("portraits") of dispersive ensembles of interest, which can be used for optimization of physical characteristics of the ensembles.

Up to now most of simulations of the statistical physical characteristics of dispersive ensembles of semiconductor nano-objects were devoted to the inhomogeneous broadening in optics of ensembles of semiconductor quantum dots. The simulations were performed for simple spherical or cubic shapes of the dots[6–9] and the broadening was attributed to the dot-size (volume) primitive univariate (single-parameter, for instance the dot radius) dispersion. This approach allows for simple analytical expressions and nonextensive numerical simulations. However, it is obviously not applicable to most of the nano-objects. The general approach to the realistic theoretical description of dispersive ensembles of semiconductor nano-objects with complex material parameters and geometrical shapes is to consider a multivariate (multidimensional) distribution function[10–12] including dispersions of all appropriate physical parameters (subsets of parameters of interest[10,13]). This requires computational methods those can optimize extensive simulations of the physical properties of semiconductor nano-objects within wide ranges of variations of their parameters. The mapping method recently proposed by us[14–16] allows one to efficiently simulate quantum-mechanical properties of ensembles of three-dimensional semiconductor nano-objects with complicated geometries and flexible material parameters.

In this theoretical study, using the mapping method we address the issue of the statistical description of the static magnetic response of dispersive ensembles of three-dimensional $In_xGa_{1-x}As/GaAs$ self-assembled quantum rings (SAQRs)—nano-objects with a very complex geometry. According to recent experimental results the SAQRs demonstrate controllable flexibility of geometrical and material characteristics (see, e.g., Refs. 5 and 17–34 and references therein). The most intriguing property of the SAQRs, that has attracted much attention, is their three-dimensional nonsimply connected topology. The property enables topological quantum effects for charged particles confined in the SAQRs (similar to the Aharonov-Bohm effect[35]). This results in a very specific static magnetic response of the rings: when the external magnetic field is applied in the SAQR growth direction, the nonsimply connected topology enables the Aharonov-Bohm oscillations of the ring's magnetization and generates a positive peak in the differential magnetic susceptibility.[36–40] This

 ©2012 American Physical Society

effect has to be addressed to the crossing between the two lowest-energy states of the electron confined in the ring.[36–42] The effect was recently experimentally confirmed at low temperatures for $In_xGa_{1-x}As/GaAs$ self-assembled capped wobbled quantum rings.[40] It was shown that for one-electron rings the wobbling asymmetry can have a strong effect on the magnitude of the first magnetization oscillation and susceptibility peak as well as their positions.[39,41] However, the actual experimental magnitude of the peak's height and its temperature dependence remain in a contradiction to the conventional expectations.[38,40–42] Unlike the conventional simulations, the experimental peak demonstrates a negligible temperature effect. In Refs. 40 and 41 the importance of the ring size variations was emphasized and it was demonstrated that the negligible temperature effect on the static magnetic response is due to the ring ensemble averaging.

In this paper we develop a "multivariate statistical portrait" of the static magnetic response for the most popular model of the geometry of three-dimensional wobbled $In_xGa_{1-x}As/GaAs$ SAQRs.[21,40] Using our mapping method we analyze conditional and simultaneous impacts of the multivariate dispersion of different geometrical properties (parameters) of the SAQRs on the first oscillation in the magnetic response of the rings' ensembles. We show that our approach makes it possible to verify which specific parameter can play a crucial role in the unusual magnetic response. In addition, we address the issue of the temperature stabilization of the static magnetic response of the dispersive ensemble of SAQRs.

II. MODEL AND SIMULATION METHODS

To make this paper more self-contained, we first briefly explain the multivariate statistics approach and its application to the simulation of the magnetic response of dispersive ensembles of nano-objects of complex geometrical shapes. We also describe the application of our mapping method to the simulation of the energy states of a single electron confined in a three-dimensional SAQR with flexible size and geometry parameters.

The geometrical and material parameters' dispersions in ensembles of nano-objects can be described by a multivariate (multidimensional) joint distribution function $P(\{x_1,x_2,\ldots,x_n\})$.[10–12] The function presents the dispersions of all appropriate parameters $\{x_i\}$ (such as sizes, parameters' characterizing anisotropy in geometry, composition, etc.). This gives the number of nano-objects dN with the values of $\{x_i\}$ inside the domain $\{x_i, x_i + dx_i\}$ as[13]

$$dN = \prod_i P(\{x_i\})dx_i. \tag{1}$$

The cumulative expectation (meaningful average) of a physical quantity $Q(\{x_i\})$ characterizing the ensemble then is written as

$$\bar{Q} = \int_{x_i} P(\{x_i\})Q(\{x_i\}) \prod_i dx_i. \tag{2}$$

Most of the ensembles can be characterized satisfactorily when only a subset of the parameters in $\{x_i\}$ is of any interest. Therefore, we can consider the conditional distributions for subsets of the parameters of interest: $\{x_j\}_C \subseteq \{x_i\}$. Accordingly, when it is possible to neglect dispersions of the other ("nuisance") parameters we can define the appropriate conditional expectation as

$$\bar{Q}_C = \int_{x_j \in \{x_j\}_C} P(\{x_j\}_C)Q(\{x_j\}_C) \prod_j dx_j. \tag{3}$$

In our consideration we assume that the parameters in a typical nano-objects' ensemble follow the noncorrelated normal distribution which is presented by

$$P(\{x_i\}) = P_G(x_1) \cdot P_G(x_2) \ldots, \tag{4}$$

where the standard normal distribution for each parameter x is written as

$$P_G(x) = AG\left(\frac{x - \bar{x}}{\triangle x}\right). \tag{5}$$

A stands for the normalization coefficient, $\bar{x}$ is a mean value, $\triangle x$ is the standard deviation of the parameter x, and $G(y)$ is the Gaussian function. Therefore, a conditional expectation (average) is

$$\bar{Q}_C = \int_{x_j \in \{x_j\}_C} Q(\{x_j\}_C) \prod_j P_G(x_j) \prod_j dx_j. \tag{6}$$

As an implementation of this statistical approach we present in this paper a conditional "statistical portrait" of the static magnetic response for the most popular model of the geometry of three-dimensional wobbled $In_xGa_{1-x}As/GaAs$ SAQRs. We start from the simulation of an individual ring and we vary the object geometrical parameters of interest within a wide range. To reach this crucial goal we use our mapping method, which allows us to map realistic geometrical shapes, strains, and material compositions of semiconductor nano-objects (known from experiments) to smooth three-dimensional effective potentials for electrons confined in the objects and very efficiently simulate the energy states of the electrons. Then we compute conditional averages of the magnetization and differential magnetic susceptibility of the rings' ensemble by using the multivariate distribution function $P(\{x_i\}_C)$.

Now we assume that a SAQR was grown on a flat substrate parallel to the x-y plane and we can model the ring's shape by a function $h(x,y)$, which reproduces the local ring's height (along the z direction) at the actual position on the x-y plane [see Fig. 1(a)]. Using the experimental structural and composition data obtained from atomic force microscopy and cross-sectional scanning tunneling microscopy measurements[21,40] the function $h(x,y)$ can be analytically approximated. For the wobbled (asymmetrical) SAQR the height $h(x,y)$ was obtained according to a fitting of the experimental data[21] and it can be written as the following (the most popular model of the

ring's geometry):

$$h(x,y)=\begin{cases} h_0+\left[h_r\left(1+\xi\frac{x^2-y^2}{x^2+y^2}\right)-h_0\right]\frac{\gamma_0^2}{R_r^2}\frac{R_r^2-(\sqrt{x^2+y^2}-R_r)^2}{(\sqrt{x^2+y^2}-R_r)^2+\gamma_0^2}, & \sqrt{x^2+y^2}\leqslant R_r \\ h_\infty+\left[h_r\left(1+\xi\frac{x^2-y^2}{x^2+y^2}\right)-h_\infty\right]\frac{\gamma_\infty^2}{(\sqrt{x^2+y^2}-R_r)^2+\gamma_\infty^2}, & \sqrt{x^2+y^2}>R_r \end{cases}, \tag{7}$$

where R_r is the ring's rim radius; h_0,h_r, and h_∞ correspondingly stand for the height at the center of the rings, at the rim, and far outside of the ring; γ_0 and γ_∞, respectively, determine the inside and outside slopes near the ring's rim. The wobbling parameter ξ defines the anisotropy (asymmetry) of the ring height on the x-y plane. The three-dimensional smooth confinement potential for electrons $V(\mathbf{r})$ we describe by the composition- and geometry-dependent profile of the local conduction-band offset:[14,16]

$$V(\mathbf{r})=\Delta E_c(\mathbf{r})=\Delta E_c^0\left(1-\frac{1}{4}\left[1+\tanh\left(\frac{z}{a}\right)\right]\times\left\{1-\tanh\left[\frac{z-h(x,y)}{a}\right]\right\}\right). \tag{8}$$

In this expression, $\mathbf{r}=(x,y,z)$ is the three-dimensional radius vector, $\Delta E_c(\mathbf{r})$ is the local value of the conduction-band offset, $\Delta {E_c}^0={E_c}^{\rm out}-{E_c}^{\rm in}$ is the overall band offset between the inner and outer semiconductor materials in the InGaAs/GaAs heterostructure, and superscripts "in" and "out" denote the actual material parameters inside and outside the rings. The slope and range (the degree of smoothness) of the potential change at the boundaries of the ring are controlled by a parameter a. The expression (8) obviously describes a rigorous full three-dimensional hard wall potential when the parameter a goes to 0. We should note that several smooth confinement potential models have been already proposed and used in simulations of semiconductor nano-objects.[43–47]

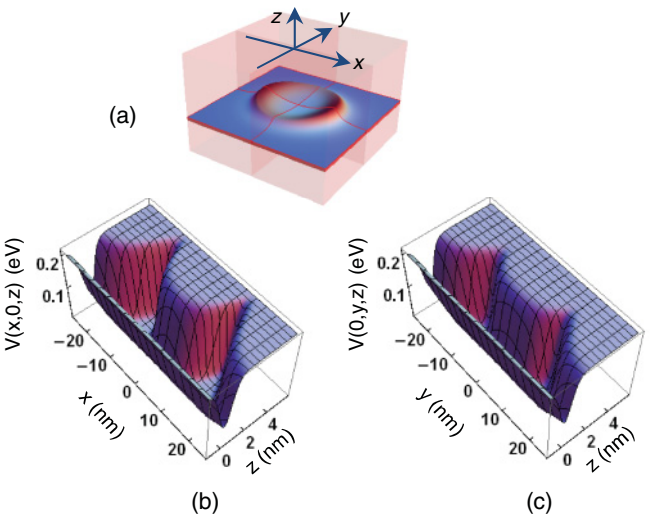

FIG. 1. (Color online) (a) Capped wobbled $In_xGa_{1-x}As/GaAs$ self-assembled quantum ring. Two projections of the electronic confinement potential on (b) $(x,0,z)$ and (c) $(0,y,z)$ planes ($R_r=11.5$ nm, $\xi=0.2$).

Specifically, following the actual three-dimensional geometrical shape of the ring, the three-dimensional confinement potential (8) reflects in a very obvious and natural way the smooth variations of the material parameters across the boundaries of the wobbled ring [see Figs. 1(b) and 1(c)].

Using the potential (8) we define the mapping function

$$M(\mathbf{r})=1-\frac{V(\mathbf{r})}{\Delta E_c^0}, \tag{9}$$

which accumulates experimental information about the ring shape and local material content. For instance, we present the position-dependent band gap $E_g(\mathbf{r})$, spin-orbit splitting $\Delta(\mathbf{r})$, the electron effective mass at the bottom of the conducting band $m_b(\mathbf{r})$ as

$$\begin{aligned} E_g(\mathbf{r})&=E_g^{\rm in}M(\mathbf{r})+E_g^{\rm out}[1-M(\mathbf{r})],\\ \Delta(\mathbf{r})&=\Delta^{\rm in}M(\mathbf{r})+\Delta^{\rm out}[1-M(\mathbf{r})],\\ m_b(\mathbf{r})&=m_b^{\rm in}M(\mathbf{r})+m_b^{\rm out}[1-M(\mathbf{r})]. \end{aligned} \tag{10}$$

Now the energy (E) and position ($\mathbf{r}$) dependent electron effective mass $m(E,\mathbf{r})$ and Landé factor $g(E,\mathbf{r})$ in the ring can be written as[36,37,48]

$$\frac{1}{m(E,\mathbf{r})}=\frac{2P^2(\mathbf{r})}{3\hbar^2}\left[\frac{2}{E+E_g(\mathbf{r})-V(\mathbf{r})}+\frac{1}{E+E_g(\mathbf{r})+\Delta(\mathbf{r})-V(\mathbf{r})}\right], \tag{11}$$

$$g(E,\mathbf{r})=2\left\{1-\frac{m_0}{m(E,\mathbf{r})}\times\frac{\Delta(\mathbf{r})}{3[E+E_g(\mathbf{r})-V(\mathbf{r})]+2\Delta(\mathbf{r})}\right\}, \tag{12}$$

where

$$P^2(\mathbf{r})=\frac{3\hbar^2}{2}m_b^{-1}(\mathbf{r})\left\{\frac{2\Delta(\mathbf{r})+3E_g(\mathbf{r})}{E_g(\mathbf{r})[E_g(\mathbf{r})+\Delta(\mathbf{r})]}\right\}^{-1}$$

presents the position-dependent momentum matrix element and m_0 is the free-electron mass.

Energy states of a single electron confined in the SAQR we can obtain in the one electronic band envelope function approximation by solving the nonlinear Schrödinger equation[36,37,48]

$$\hat{H}(E,\mathbf{r})F(\mathbf{r})=EF(\mathbf{r}) \tag{13}$$

with the effective energy-dependent Hamiltonian

$$\hat{H}(E,\mathbf{r})=\frac{1}{2}\Pi_{\mathbf{r}}\frac{1}{m(E,\mathbf{r})}\Pi_{\mathbf{r}}+\frac{\mu_B}{2}g(E,\mathbf{r})\sigma\cdot\mathbf{B}+V(\mathbf{r}), \tag{14}$$

where $\Pi_{\mathbf{r}}=-i\hbar\nabla_{\mathbf{r}}+e\mathbf{A}(\mathbf{r})$ is the electron momentum operator, $\nabla_{\mathbf{r}}$ is the spatial gradient, $\mathbf{A}(\mathbf{r})$ is the vector potential of the

magnetic field $\mathbf{B} = \nabla \times \mathbf{A}$, σ is the vector of the Pauli matrices, μ_B is the Bohr magneton, and e is the elementary charge.

To determine the ring's static magnetic response we first calculate the magnetic moment M (magnetization) of an electron localized in a ring. The standard approach for arbitrary temperature T is to use the free energy F of the system in the presence of the external magnetic field $\mathbf{B}$:[49,50]

$$F = -k_B T \ln Z, \tag{15}$$

where the single-particle partition function Z is defined to be

$$Z = \sum_n \exp\left(-\frac{E_n}{k_B T}\right), \tag{16}$$

and the energy states are numerated by $\{n\}$—an appropriate set of quantum numbers must be obtained by the solution of Eq. (13). Then, the single-electron magnetization M and differential magnetic susceptibility χ of a ring are correspondingly

$$M = \frac{1}{Z}\sum_n \left(-\frac{\partial E_n}{\partial B}\right)\exp\left(-\frac{E_n}{k_B T}\right) \tag{17}$$

and

$$\chi = \frac{\partial M}{\partial B}. \tag{18}$$

At low temperatures the magnetization and susceptibility of a ring are defined by the magnetic-field dependencies of the lowest-energy states. It is known[36–40] that the first oscillation of the magnetization and correspondingly the first positive peak of the susceptibility appear at the crossing of the ground E_0 and first excited E_1 electron energy levels (manifesting the Aharonov-Bohm effect). Therefore, for clarity in this paper we concentrate on the first oscillation of the magnetic parameters of the rings. At the neighborhood of the crossing point B_c we can suggest that (see also as an illustration Fig. 2)

$$\begin{aligned} E_{0(1)}(B) &\approx E_c + C_{0(1)}(B - B_c), \\ E_c &= E_0(B_c) = E_1(B_c). \end{aligned} \tag{19}$$

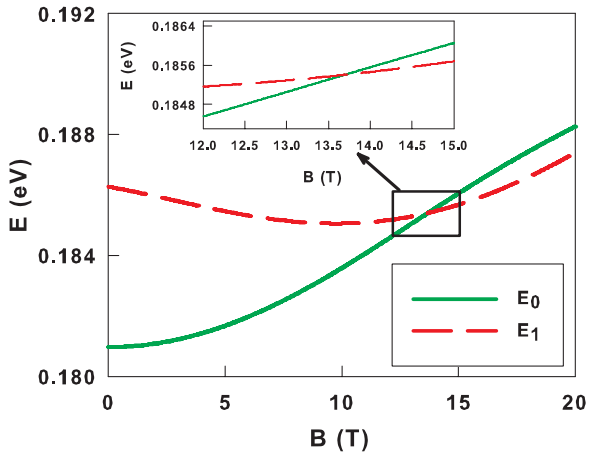

FIG. 2. (Color online) Two lowest electron energy levels for the ring with $R_r = 11.5$ nm and $\xi = 0.2$. Inset: crossing region.

We stress that at low temperatures near the crossing point B_c the two lowest levels can be properly separated from the higher-energy levels[36,37,39,40] and we can keep in Z only two terms. In this approximation, the magnetization Eq. (17) and differential magnetic susceptibility Eq. (18) can be written as

$$M \approx -\frac{C_0 - C_1 \exp\delta}{1 + \exp\delta} \tag{20}$$

and

$$\chi \approx \frac{(C_0 - C_1)^2}{k_B T}\cdot\frac{\exp\delta}{(1+\exp\delta)^2}, \tag{21}$$

where

$$\delta = \frac{(C_0 - C_1)(B - Bc)}{k_B T}.$$

Actual values of the electronic energies near the first crossing, amplitudes of the magnetization oscillation, and susceptibility peak [defined in Eqs. (20) and (21) by B_c and $C_{0(1)}$] strongly depend on the actual geometrical and material parameters of the rings such as effective radii, heights, material content, strain, etc.[21,36,37,39,40] Therefore, in general, within our approach we can characterize them by a set of parameters $\{x_i\} \Rightarrow \{R_r, \xi, h_0, h_r \ldots, \Delta E_c^0, E_g^{\text{in(out)}}, m_b^{\text{in(out)}} \ldots\}$ [see, e.g., Eqs. (1)–(10)]. From an experiment one actually obtains values of the magnetic characteristics averaged over an ensemble of the rings with dispersions of certain selected parameters combined into the conditional set $\{x_i\}_C$. The meaningful averages for the magnetization and differential magnetic susceptibility characterizing the ensemble can be written as

$$\bar{M}_C = \int\limits_{x_j \in \{x_j\}_C} M(\{x_j\}_C) \prod_j P_G(x_j) \prod_j dx_j, \tag{22}$$

$$\bar{\chi}_C = \int\limits_{x_j \in \{x_j\}_C} \chi(\{x_j\}_C) \prod_j P_G(x_j) \prod_j dx_j. \tag{23}$$

We note that in our description near the crossing point the ring parameter variations within an ensemble of the rings are obviously connected with the variations of $B_c(\{x_i\})$ and $C_{0(1)}(\{x_i\})$; those according to Eqs. (21) and (22) we have to model in the first place.

III. SIMULATION RESULTS AND DISCUSSION

The larger the conditional set of varying parameters $\{x_i\}_C \Rightarrow \{R_r, \xi, h_0, h_r \ldots, \Delta E_c^0, E_g^{\text{in(out)}}, m_b^{\text{in(out)}} \ldots\}_C$, the more complete "statistical portrait" of the magnetic response of the rings' ensemble can be drawn and the more complete description for $\overline{M}$ and $\overline{\chi}$ can be proposed. According to the general scheme we have to simulate multidimensional dependencies of the coefficients $B_c(\{x_i\}_C)$ and $C_{0(1)}(\{x_i\}_C)$. However, it is already a tedious problem itself to solve many times the three-dimensional nonlinear Schrödinger equation (13) for varying combinations of the values of the parameters from a conditional subset and changing magnetic field (which is parallel to the z direction). Therefore, we consider only $In_xGa_{1-x}As/GaAs$ SAQRs and use realistic semiconductor material parameters $\{\Delta E_c^0, E_g^{\text{in(out)}}, m_b^{\text{in(out)}} \ldots\}_C$ for

InGaAs/GaAs heterostructures known from Refs. 51–53 and adjusted according to the actual composition and strain.[21,39,40] We take them as fixed parameters without dispersion and focus on the pure geometry dispersion. To decrease the problem complicity we consider the magnetic-field range corresponding to the first oscillation of the magnetization and the first positive peak of the susceptibility. For this reason we should select from the conditional geometrical subset $\{R_r,\xi,h_0,h_r\ldots\}_C$ only those parameters whose variations are relevant to the main changes in the position of the crossing point and values of C_0 and C_1. We have to keep the parameters' variations within certain bars to guarantee the appearance of the crossing and oscillations. Therefore, in this paper we confine ourselves to a bivariate (two-dimensional) distribution for the variations in Eq. (1) when only the parameters R_r and ξ vary (the conditional subset $\{R_r,\xi\}_C$). According to Refs. 39 and 41 and our calculation experience, dispersions (up to 20%) of these two parameters for the wobbled rings with geometry Eq. (1) are most relevant for the deviation in the crossing point B_c position. With conditions described above the dispersion of other geometrical parameters plays a less important role and will be considered elsewhere. Using Eq. (1) and solving Eq. (13) we first simulate $E_{0(1)}(B;\{R_r,\xi\}_C)$ in the vicinity of the crossing point. The energy states are obtained numerically from solutions of the full three-dimensional eigenvalue problem Eq. (13) using the nonlinear iterative method[54] and the COMSOL finite element analysis, solver, and simulation software.[55]

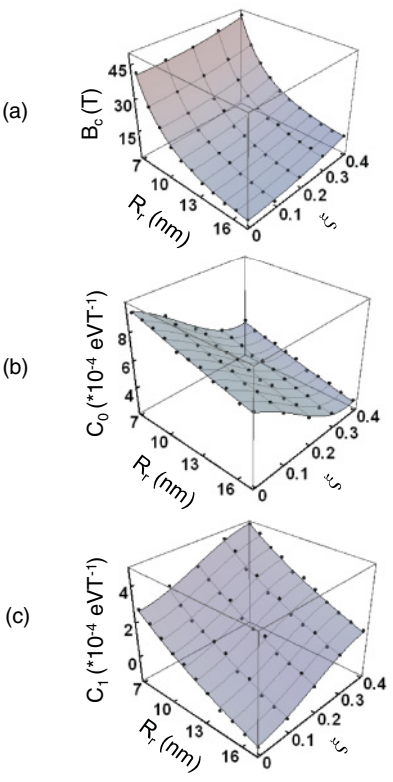

FIG. 3. (Color online) Dependencies of the electronic energy characteristics on the rim radius R_r and wobbling parameter ξ: (a) crossing point B_c, (b) coefficient C_0, and (c) coefficient C_1. Dots, simulation data; surface plots, appropriate fitting functions.

TABLE I. Fitting parameters.

k	0	1	c
a_k	1.209×10^{-3}	2.131×10^{-3}	0
b_k	-9.164×10^{-4}	1.659×10^{-4}	1.058
c_k	-4.743×10^{-3}	3.059×10^{-3}	36.96
d_k	1.069×10^{-3}	-5.115×10^{-3}	0
e_k	-6.544×10^{-5}	-1.247×10^{-3}	5222.2
β_k	0.722	0.206	−2.491

By adjusting the model presented by Eq. (1), we adopt the experimental data[21,40] and choose a basic geometrical shape of the rings (known from the experiment) as follows: $h_0 = 1.6$ nm, $h_r = 3.6$ nm, and $h_\infty = 0.4$ nm, $\gamma_0 = 5$ nm, and $\gamma_\infty = 2$ nm. The slope parameter of the potential change at the boundaries of the rings is chosen to be $a = 0.4$ nm. As an example, two different projections of the smooth three-dimensional confinement potential of the ring with $R_r = 11.5$ nm, $\xi = 0.2$ are shown in Figs. 1(b) and 1(c), and the first crossing of the electronic energy levels for this ring is presented in Fig. 2. In our simulations the parameters R_r and ξ are varied within the ranges 7−17 nm and 0−0.4, correspondingly. Values of $B_c(\{R_r,\xi\}_C)$ and $C_{0(1)}(\{R_r,\xi\}_C)$ are reproduced from the calculation results for the corresponding sets $\{R_r,\xi\}_C$ (see Fig. 3). The results of those simulations we fit to the two-dimensional functions $C_{0(1)}(\{R_r,\xi\}_C)$ and $B_c(\{R_r,\xi\}_C)$ using the following guess:

$$X_k(R_r,\xi) = a_k + b_k\xi + c_k\xi^2 + d_k\xi^3 + e_k R_r^{\beta_k}, \qquad (24)$$

where $k = 0,1,c$ and $X_k(R_r,\xi) = (C_0,C_1,B_c)$. According to our experience, the best fit can be achieved with the fitting parameters in Eq. (24) given in Table I (in appropriate International System units).

It is clear from Fig. 3 that the fitting functions $B_c(R_r,\xi)$ and $C_{0(1)}(R_r,\xi)$ accurately reproduce results of our direct simulation within the chosen wide range of variations of the parameters. Clearly, within the fitting range the variations of the ring rim radius strongly affect the position of the crossing point, which also demonstrates a relatively weak dependence on the wobbling parameter ξ [Fig. 3(a)]. We should note that according to Eqs. (20) and (21) for a particular individual ring at low temperatures the magnitudes of the magnetization and susceptibility oscillations are defined by the difference $C_0 - C_1$ that we show in Fig. 4. Although the coefficients C_1

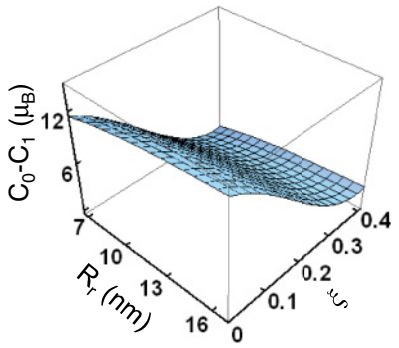

FIG. 4. (Color online) Two-dimensional dependence of the fitted difference $C_0 - C_1$ on the rim radius R_r and wobbling parameter ξ.

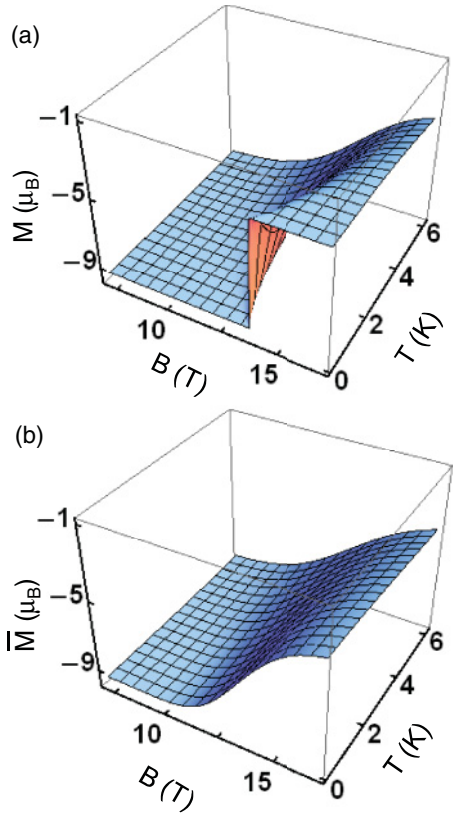

FIG. 5. (Color online) Dependence of the magnetization M on the temperature and magnetic field for (a) individual ring ($R_r = 11.5$ nm, $\xi = 0.2$) and (b) rings' ensemble ($\bar{R}_r = 11.5$ nm, $\bar{\xi} = 0.2$, dispersion 5%).

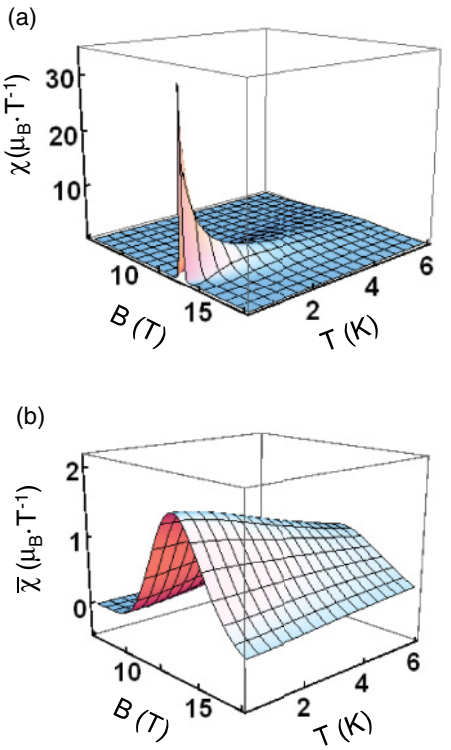

FIG. 6. (Color online) Dependence of the differential magnetic susceptibility χ on the temperature and magnetic field for (a) individual ring ($R_r = 11.5$ nm, $\xi = 0.2$) and (b) ring ensemble ($\bar{R}_r = 11.5$ nm, $\bar{\xi} = 0.2$, dispersion 5%).

and C_2 separately vary substantially as functions of both R_r and ξ [Figs. 3(b) and 3(c)], it is clear that the difference of the coefficients is very stable upon the rim radius changes, but it can be seriously affected by variations of ξ. This suggests the same tendency for the magnetization oscillations for an individual ring at low temperatures.

Substituting $B_c(R_r,\xi)$ and $C_{0(1)}(R_r,\xi)$ from Eq. (24) to Eqs. (20)–(23) we are now able to simulate the conditional meaningful averages for the magnetization and differential magnetic susceptibility characterizing dispersive ensembles of one-electron $In_xGa_{1-x}As/GaAs$ SAQRs and compare that with magnetic properties of an individual ring and the actual experimental data.

Figures 5 and 6 show results of our simulation for the temperature-dependent magnetization and differential magnetic susceptibility of an individual $In_xGa_{1-x}As/GaAs$ ring with $R_r = 11.5$ nm and $\xi = 0.2$ and the same values averaged within the ensembles of the rings with the mean values $\bar{R}_r = 11.5$ nm, $\bar{\xi} = 0.2$ when the geometrical parameter dispersions are taken to be 5% both for R_r and ξ (like it was suggested in Ref. 40). Clearly, for the individual SAQR at very low temperatures the magnetization rapidly oscillates [Fig. 5(a)] and the differential magnetic susceptibility demonstrates a very sharp symmetrical positive peak [Fig. 6(a)] near the crossing point. The magnetization oscillation and magnetic susceptibility peak amplitudes are controlled by the difference $C_0 - C_1$ and the temperature fluctuations (homogeneous broadening). The oscillation and peak become wider and disappear very rapidly when the temperature increases. This is in contrast to the experimental data from Ref. 40, where the relatively wide peak reveals itself even when the temperature increases. The temperature stable magnetization oscillation and temperature stable wide peak (inhomogeneous broadening) of the

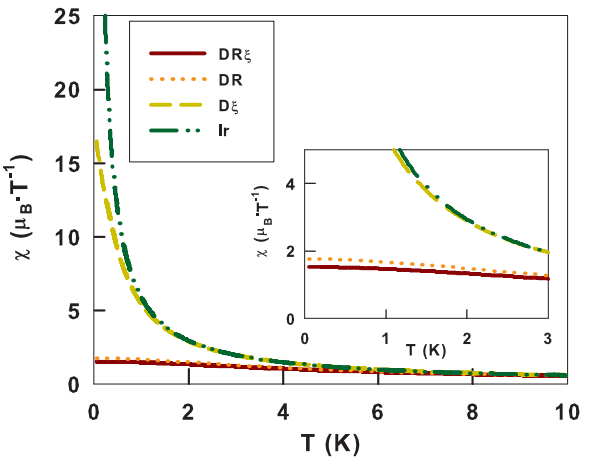

FIG. 7. (Color online) Temperature dependence of the height of the peak of the magnetic susceptibility (inset: small temperature region). DRξ, DR, Dξ, and Ir correspondingly stand for conditional bivariate dispersion of R_r and ξ ($\bar{R}_r = 11.5$ nm, $\bar{\xi} = 0.2$, dispersion 5%), univariate dispersion of R_r ($\bar{R}_r = 11.5$ nm, dispersion 5%, $\xi = 0.2$), univariate dispersion of ξ ($R_r = 11.5$ nm, $\bar{\xi} = 0.2$, dispersion 5%), and individual ring with $R_r = \bar{R}_r$, $\xi = \bar{\xi}$.

differential magnetic susceptibility indeed can be explained only by the geometry dispersion in the ring ensembles even if the dispersions are taken to be only 5%. To demonstrate that, in Figs. 5(b) and 6(b) we present the simulation results for the conditional averages of the magnetization and magnetic susceptibility of the ensemble of the rings with $\bar{R}_r = 11.5$ nm and $\bar{\xi} = 0.2$. Our conditional multivariate approach allows us to clarify which parameter's fluctuations are most relevant to the temperature stabilization of the differential magnetic susceptibility of the chosen model of the geometry of the wobbled $In_xGa_{1-x}As/GaAs$ SAQRs. In Fig. 7 we show the temperature dependence of the conditional averages of the height of the positive peak of the magnetic susceptibility (at the crossing point B_c) when two parameters (R_r and ξ) are varying separately and simultaneously while $\bar{R}_r = 11.5$ nm and $\bar{\xi} = 0.2$. Clearly, within the low-temperature range, in this ensemble the broadening due to the ring's rim radius variation [the crossing point deviations; see Fig. 3(a)] plays a crucial role in the overall inhomogeneous broadening and temperature stability of the positive peak of the differential magnetic susceptibility. At relatively high temperatures, both the homogeneous and inhomogeneous broadenings equivalently contribute to the peak height's temperature dependence.

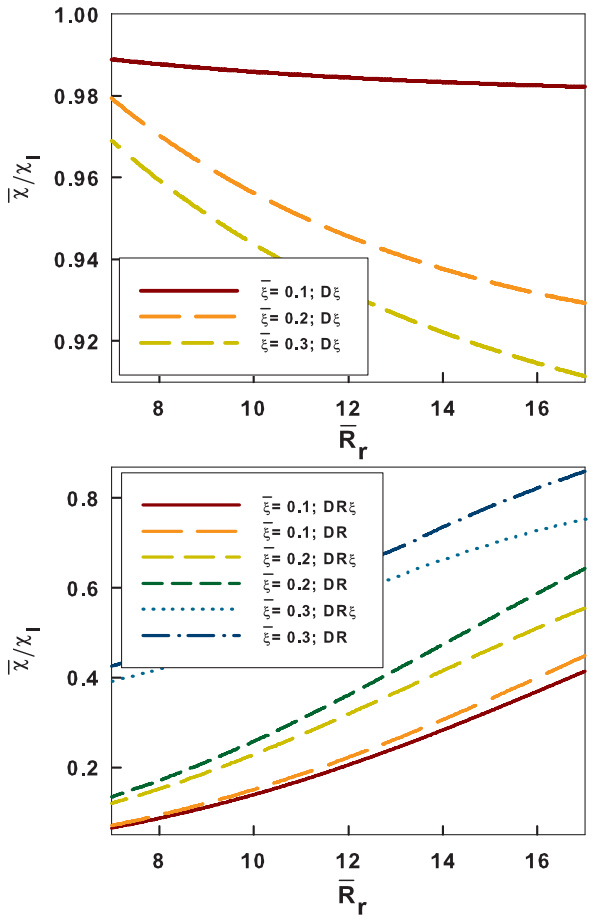

FIG. 8. (Color online) Dependence of the height of the peak of the averaged magnetic susceptibility on $\bar{R}_r$ for different $\bar{\xi}$ (normalized to the corresponding height of the individual ring χ_I with $R_r = \bar{R}_r$ and $\xi = \bar{\xi}$, dispersion 5%, $T = 1.2$ K). For descriptions of the abbreviations DRξ, DR, Dξ, see Fig. 7.

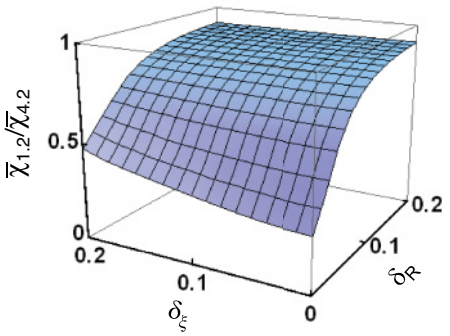

FIG. 9. (Color online) Dependence of the height-to-height ratio for the averaged peaks of the magnetic susceptibility at 1.2 K ($\bar{\chi}_{1.2}$) and 4.2 K ($\bar{\chi}_{4.2}$) on $\delta_R = \Delta R_r/\bar{R}_r$ and $\delta_\xi = \Delta\xi/\bar{\xi}$ ($\bar{R}_r = 11.5$ nm and $\bar{\xi} = 0.2$).

Now we discuss the roles of variations of the conditional parameters in the formation of the conditional average of the magnetic susceptibility near the peak position for different ensembles of the rings. Using the appropriate data shown in Figs. 3 and 4 we present in Fig. 8 the normalized conditional averages of the peak height at $T = 1.2$ K within a wide range of the ring's parameters. This information clearly suggests that for relatively small mean values of the ring radius and wobbling parameter the dispersion of the rim radius plays a major role and strongly suppresses the peak magnitude. At the same time the average height becomes closer to that for the individual ring when $\bar{R}_r$ and $\bar{\xi}$ increase. We note that according to Fig. 4 the response of the individual ring for relatively large $\bar{\xi}$ is small. However, the joint conditional average of the peak magnitude can be optimized with an appropriate control of $\bar{R}_r$ and $\bar{\xi}$.

Finally, in Fig. 9 we present a wider view of the R_r and ξ dispersions' impact on the temperature stabilization of the magnetic response of dispersive ensembles of the ring for conditional $\bar{R}_r = 11.5$ nm and $\bar{\xi} = 0.2$. For both $\delta_R = \Delta R_r/\bar{R}_r$ and $\delta_\xi = \Delta\xi/\bar{\xi}$ the dispersion interval expansion obviously stabilizes the temperature characteristics of the response. In general, for a large dispersion the stabilization is achieved at small values of the peak magnitudes. At the same time an appropriate δ_ξ can make the ensemble magnetic characteristics more tolerant to the deviations of R_r (see Fig. 9). The optimization of the ensemble characteristics by a proper control of $\bar{R}_r$ and $\bar{\xi}$ gives us an opportunity to design an ensemble of the rings with a large enough and temperature stable peak in the collective magnetic response.

IV. CONCLUSIONS

In conclusion, using the multivariate (multidimensional) statistics approach and our mapping method we simulated the static magnetic response of dispersive ensembles of self-assembled semiconductor quantum rings with complicated (wobbled) shapes. The approach can be used for systems with large sets of varying parameters. In this paper we obtained conditional averages of the magnetization and differential magnetic susceptibility near the first Aharonov-Bohm oscillation and analyzed the averaged properties within a wide range of changes of rings' geometrical parameters. We

should note that, using our multivariate approach, we are able to draw a conditional "statistical portrait" of the magnetic response of the ensembles. This makes it possible to clarify the important question of which geometrical parameters' dispersions are crucial for the formation and properties of the magnetic response of ensembles of self-assembled semiconductor quantum rings. Therefore, our simulation results for the $In_xGa_{1-x}As/GaAs$ SAQRs within a bivariate geometrical dispersion model suggest directions to the optimization of the unusual static magnetic response for dispersive ensembles of the rings.

In addition, we addressed in detail the issue of the temperature stable behavior of the meaningful averages of the magnetization and positive differential magnetic susceptibility known from the experiment.[40] The simulated position and the magnitude of the positive peak in the differential magnetic susceptibility are in good agreement with the experimental observations. The negligible temperature effect on the magnetic response of the rings is preferably caused by dispersion of the ring's rim radius in the ensemble. We suggest that the optimization of the rings' characteristics can help to design ensembles of the rings with large enough and temperature stable unusual collective magnetic response. This can be potentially useful for further fabrication of composite systems (metamaterials) with principally new magnetic properties.

More generally, the conditional multivariate approach can be applied for the realistic modeling of the meaningful averages of the response functions for dispersive ensembles of semiconductor nano-objects with arbitrary shapes.

ACKNOWLEDGMENTS

This work is supported by the National Science Council of the Republic of China, under Contracts No. NSC 100-2112-M-009-009 and No. NSC 100-2120-M-009-005, and by the "Aim for the Top University Plan" of the National Chiao Tung University and Ministry of Education of Taiwan, Republic of China.

*Corresponding author: vam@faculty.nctu.edu.tw

[1] *Semiconductor Nanostructures*, edited by D. Bimberg (Springer, Berlin, 2008).
[2] G. Konstantatos and E. H. Sargent, Nature Nanotechnology **5**, 391 (2010).
[3] M. Yamagiwa, T. Mano, T. Kuroda, T. Tateno, K. Sakoda, G. Kido, N. Koguchi, and F. Minami, Appl. Phys. Lett. **89**, 113115 (2006).
[4] J. He, R. Nötzel, P. Offermans, P. M. Koenraad, Q. Gong, G. J. Hamhuis, T. J. Eijkemans, and J. H. Wolter, Appl. Phys. Lett. **85**, 2771 (2004).
[5] J. M. García, G. Medeiros-Ribeiro, K. Schmidt, T. Ngo, J. L. Feng, A. Lorke, J. Kotthaus, and P. M. Petroff, Appl. Phys. Lett. **71**, 2014 (1997).
[6] V. I. Belyavskii and S. V. Shevtsov, Semiconductors **36**, 821 (2002).
[7] V. V. Nikolaev and N. S. Averkiev, Appl. Phys. Lett. **95**, 263107 (2009).
[8] D. L. Ferreira and J. L. A. Alves, Nanotechnology **15**, 975 (2004).
[9] V. Kumar and D. Biswas, J. Appl. Phys. **102**, 084305 (2007).
[10] A. C. Rencher, *Methods of Multivariate Analysis*, 2nd ed. (Wiley-Interscience, New York, 2002).
[11] W. Härdle and L. Simar, *Applied Multivariate Statistical Analysis*, 2nd ed. (Springer, Berlin, 2002).
[12] G. Casella and R. L. Berger, *Statistical Inference*, 2nd ed. (Duxbury, Pacific Grove, 2002).
[13] L. M. Thu, W. T. Chiu, and O. Voskoboynikov, Phys. Rev. B **83**, 125301 (2011).
[14] L. M. Thu and O. Voskoboynikov, AIP Conf. Proc. **1233**, 952 (2010).
[15] L. M. Thu, W. T. Chiu, Shao-Fu Xue, Ta-Chun Lin, and O. Voskoboynikov, Physics Procedia **3**, 1149 (2010).
[16] L. M. Thu and O. Voskoboynikov, Physics Procedia **3**, 1133 (2010).
[17] A. Lorke, R. J. Luyken, A. O. Govorov, J. P. Kotthaus, J. M. García, and P. M. Petroff, Phys. Rev. Lett. **84**, 2223 (2000).
[18] R. J. Warburton, C. Schäflein, D. Haft, F. Bickel, A. Lorke, K. Karrai, J. M. García, W. Schoenfield, and P. M. Petroff, Physica E **9**, 124 (2001).
[19] J. Cui, Q. He, X. M. Jiang, Y. L. Fan, X. J. Yang, F. Xue, and Z. M. Jiang, Appl. Phys. Lett. **83**, 2907 (2003).
[20] S. Kobayashi, C. Jiang, T. Kawazu, and H. Sakaki, Jpn. J. Appl. Phys. B **43**, L662 (2004).
[21] P. Offermans, P. M. Koenraad, J. H. Wolter, D. Granados, J. M. García, V. M. Fomin, V. N. Gladilin, and J. T. Devreese, Appl. Phys. Lett. **87**, 131902 (2005).
[22] T. Mano, T. Kuroda, S. Sanguinetti, T. Ochiai, T. Tateno, J. Kim, T. Noda, M. Kawabe, K. Sakoda, G. Kido, and N. Koguchi, Nano Lett. **5**, 425 (2005).
[23] J. Sormunen, J. Riikonen, M. Mattila, J. Tiilikainen, M. Sopanen, and H. Lipsanen, Nano Lett. **5**, 1541 (2005).
[24] F. Ding, L. Wang, S. Kiravittaya, E. Müller, A. Rastelli, and O. G. Schmidt, Appl. Phys. Lett. **90**, 173104 (2007).
[25] C. Zhao, Y. H. Chen, B. Xu, C. G. Tang, Z. G. Wang, and F. Ding, Appl. Phys. Lett. **92**, 063122 (2008).
[26] J. H. Lee, Z. M. Wang, M. E. Ware, K. C. Wijesundara, M. Garrido, E. A. Stinaff, and G. J. Salamo, Crystal Growth and Design **8**, 1945 (2008).
[27] R. Timm, A. Lenz, H. Eisele, L. Ivanova, M. Dähne, G. Balakrishnan, D. L. Huffaker, I. Farrer, and D. A. Ritchie, J. Vac. Sci. Technol. B **26**, 1492 (2008).
[28] V. Baranwal, G. Biasiol, S. Heun, A. Locatelli, T. O. Mentes, M. N. Orti, and L. Sorba, Phys. Rev. B **80**, 155328 (2009).
[29] J. Chen, W. S. Liao, X. Chen, T. Yang, S. E. Wark, D. H. Son, J. D. Batteas, and P. S. Cremer, ACS Nano **3**, 173 (2009).
[30] T. C. Lin, C. H. Lin, H. S. Ling, Y. J. Fu, W. H. Chang, S. D. Lin, and C. P. Lee, Phys. Rev. B **80**, 081304(R) (2009).
[31] C.-H. Lee, C. W. Liu, H.-T. Chang, and S. W. Lee, J. Appl. Phys. **107**, 056103 (2010).
[32] S. Sanguinetti, C. Somaschini, S. Bietti, and N. Koguchi, Nanomater. Nanotechnol. **1**, 14 (2011).

[33]P. Moon, W. J. Choi, K. Park, E. Yoon, and J. D. Lee, J. Appl. Phys. **109**, 103701 (2011).
[34]F. Ding, B. Li, N. Akopian, U. Perinetti, Y. H. Chen, F. M. Peeters, A. Rastelli, V. Zwiller, and O. G. Schmidt, J. Nanoelectron. Optoelectron. **6**, 51 (2011).
[35]Y. Aharonov and D. Bohm, Phys. Rev. **115**, 485 (1959).
[36]O. Voskoboynikov, Y. Li, H. M. Lu, C. F. Shih, and C. P. Lee, Phys. Rev. B **66**, 155306 (2002).
[37]J. I. Climente, J. Planelles, and J. L. Movilla, Phys. Rev. B **70**, 081301(R) (2004).
[38]O. Voskoboynikov and C. P. Lee, Physica E **20**, 278 (2004).
[39]P. Offermans, P. M. Koenraad, J. H. Wolter, D. Granados, J. M. García, V. M. Fomin, V. N. Gladilin, and J. T. Devreese, Physica E **32**, 41 (2006).
[40]N. A. J. M. Kleemans, I. M. A. Bominaar-Silkens, V. M. Fomin, V. N. Gladilin, D. Granados, A. G. Taboada, J. M. García, P. Offermans, U. Zeitler, P. C. M. Christianen, J. C. Maan, J. T. Devreese, and P. M. Koenraad, Phys. Rev. Lett. **99**, 146808 (2007).
[41]V. M. Fomin, V. N. Gladilin, S. N. Klimin, J. T. Devreese, N. A. J. M. Kleemans, and P. M. Koenraad, Phys. Rev. B **76**, 235320 (2007).
[42]V. M. Fomin, V. N. Gladilin, J. T. Devreese, N. A. J. M. Kleemans, and P. M. Koenraad, Phys. Rev. B **77**, 205326 (2008).
[43]B. Szafran, S. Bednarek, and J. Adamowski, Phys. Rev. B **64**, 125301 (2001).
[44]D. Chaney, M. Roy, and P. Maksym, in *Quantum Dots: Fundamentals, Applications, and Frontiers*, edited by B. A. Joyce, P. C. Kelires, A. G. Naumovets, and D. D. Vvedensky (Springer, Dordrecht, 2005), p. 239.
[45]V. Mlinar, A. Schliwa, D. Bimberg, and F. M. Peeters, Phys. Rev. B **75**, 205308 (2007).
[46]G. E. Cragg and A. L. Efros, Nano Lett. **10**, 313 (2010).
[47]R. Vaxenburg and E. Lifshitz, Phys. Rev. B **85**, 075304 (2012).
[48]G. Bastard, *Wave Mechanics Applied to Semiconductor Heterostructures* (Edition de Physique, Les Ulis, 1990).
[49]R. P. Feynman, *Statistical Mechanics: A Set of Lectures* (Westview, Boulder, 1998).
[50]N. Majlis, *The Quantum Theory of Magnetism*, 2nd ed. (World Scientific, Singapore, 2007).
[51]I. Vurgaftman, J. R. Meyer, and L. R. Ram-Mohan, J. Appl. Phys. **89**, 5815 (2001).
[52]C. E. Pryor and M. E. Pistol, Phys. Rev. B **72**, 205311 (2005).
[53]O. Voskoboynikov, Phys. Rev. B **78**, 113310 (2008).
[54]Y. M. Li, O. Voskoboynikov, C. P. Lee, and S. M. Sze, Comput. Phys. Commun. **141**, 66 (2001).
[55]See www.comsol.com.